Development of Multipath Mitigation Methods to Improve GNSS Positioning Accuracy Under Urban Environments

FUKUZAKI Yoshihiro, ONAKA Yasuhiko, TADA Naohiro, MIYAGAWA Kohei, SAKAI Kazuki, FURUYA Tomoaki, KAMAKARI Yuki, YAMAO Hiromi, HIYAMA Yohei and HATANAKA Yuki

(Published online: 30 October 2019)

Abstract

The accuracy of Global Navigation Satellite System (GNSS) positioning is easily degraded under severe environments such as urban street surroundings due to the blockage of satellite signals by tall buildings. One of the causes of GNSS positioning accuracy degradation is the multipath effect, a phenomenon known to occur in urban areas. To improve the positioning accuracy under such environments, we developed three new methods for multipath mitigation by employing promising techniques from previous studies. The first is the application of an elevation cutoff mask model produced from the distribution data of area obstacles causing the blockage of GNSS signals. The distribution at each site is identified from photos of an overhead sky (e.g. fisheye lens photos), and the elevation cutoff mask model for each site is individually produced and applied to eliminate non-line-of-sight satellites. The second is the application of another elevation cutoff mask model produced from the distribution data of buildings identified from a 3D map. The third is a quality check of the observation data utilizing L1 and L2 Doppler observables. If the observation data contain undesirable signals such as multipath signals, the difference between the L1 and L2 Doppler observables will not agree with the difference in the case of only true signals. By using the discrepancy detected with the Doppler observables, the data can be rejected as invalid observations. These three methods allow observers to select the proper satellites with greater certainty and perform more accurate positioning by identifying the observation data to be rejected. This paper presents the development results of the new methods.

1. Introduction

Realization and popularization of the Global Navigation Satellite System (GNSS) including the Global Positioning System (GPS) developed and maintained by the United States and the Quasi-Zenith Satellite System (QZSS) by Japan has made daily life much safer and more convenient. Life without the use of GNSS devices such as automobile navigation systems and smartphones is no longer imaginable.

The accuracy of GNSS positioning, however, is easily degraded under severe environments such as urban street surroundings. For example, tall buildings block the GNSS satellite signals, which should be received at the positioning point. In addition, undesirable signals that are reflected or diffracted by the buildings are received together with the true signals coming directly from the satellites. This is known as the 'multipath effect' (Fig. 1). Contamination of the true signals with multipath signals results in degradation of the GNSS positioning accuracy.

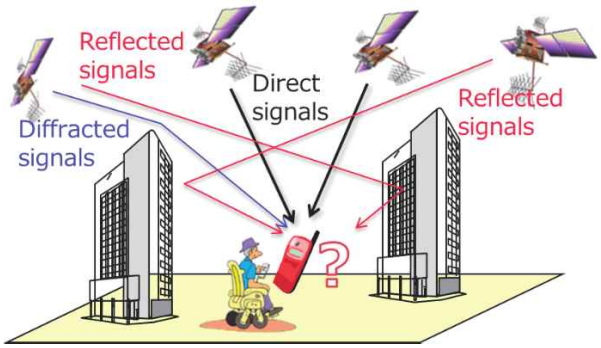

Fig. 1 Multipath effect under urban environments

Since 1996, the Geospatial Information Authority of Japan (GSI) has installed and maintained Continuously Operating Reference Stations (CORSs) to receive GNSS signals in Japan, and the total number of stations currently exceeds 1,300 (Tsuji et al., 2017). GSI's CORS network is now called GEONET (GNSS Earth Observation Network system). By using GEONET data, especially in real time, several types of location-based services are available in Japan.

GSI is also investigating and evaluating new

technologies to improve the GNSS positioning accuracy, especially under urban environments. From 2015 to 2017, as part of a technical development project, we developed three new methods for multipath mitigation based on promising techniques from previous studies.

In this paper, we introduce the three multipath mitigation methods and report the results of trial observations to verify the developed methods.

2. Project

The three-year project "Technical Development for Realization of a Safe and Convenient Society Applying Three-Dimensional Geospatial Information" was funded as a general technical development project by the Ministry of Land, Infrastructure, Transport and Tourism in 2014, and conducted by GSI from April 2015 to March 2018 on several themes related to three-dimensional geospatial information. One of the themes was the technical development of multipath mitigation with the goal of expanding the applicable area in urban environments for GNSS precise positioning (Fukuzaki et al., 2017).

In this project, three multipath mitigation methods were developed as follows:

Method 1: Cutoff mask model produced by using a fisheye lens photo (fisheye lens photo method)

Method 2: Quality check of observation data by using Doppler observables (Doppler observable method)

Method 3: Cutoff mask model produced by using a three-dimensional map (3D map method)

3. Multipath Mitigation Methods

3.1 Method 1: Fisheye lens photo method

Under urban environments, the multipath signals reflected or diffracted by tall buildings are usually recognized by the GNSS receiver as actual signals from the proper satellite, and the true signals coming directly from the satellite do not reach the GNSS receiver because they are blocked by the buildings.

By using the visibility information of the GNSS satellites in the sky, an elevation cutoff mask model that shows the non-receivable satellites at the site is produced, and by rejecting the satellites that are not in the line of sight, the data containing the multipath signals can be eliminated. For example, photos taken by a fisheye lens at the positioning site are applied to produce the elevation cutoff mask model (Suzuki et al., 2011). In this method, the fisheye lens photo, an example of which is shown in Photo 1, is employed to produce the cutoff mask model for elimination of the multipath signals. Examples of the mask and the mask model produced with the fisheye lens photo are shown in Figs. 2 and 3, respectively.

Photo 1 Example of fisheye lens photo

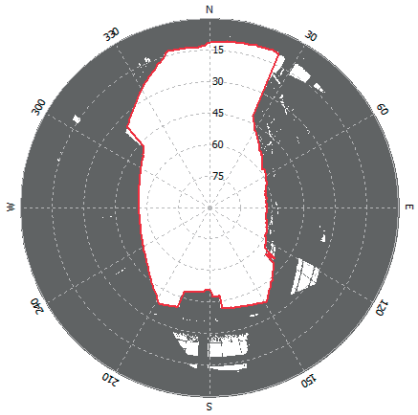

Fig. 2 Example of mask produced with fisheye lens photo (After adjustment of photo orientation and distortion)

3.2 Method 2: Doppler observable method

The Doppler shift of the received signal is detected by the GNSS receiver since the GNSS satellite is relatively moving to the receiver. The amount of Doppler shift is calculated by the equation:

$$f = f_0 \times \frac{\sqrt{1-\left(V/c\right)^2}}{1-\left(V/c\right)\cos\theta}$$

where f is the shifted frequency, f_0 is the original frequency, V is the relative velocity of the satellite, c is the speed of light, and θ is the angle of the two directions of the emitted signal and the satellite orbit. Since there is a difference in the relative velocity of the satellite between the true and multipath signals, the amount of Doppler shift for the multipath signal is different from that of the true signal. If the observation data contain the multipath signals, the difference between the L1 and L2 Doppler observables will not agree with the difference in the case of only true signals, and by detecting this discrepancy, the data containing the multipath signal can be rejected as invalid observations.

```
% Elevation Mask
% AZ(deg) EL(deg)
    0.0   12.0
    2.0   11.8
    3.0   11.7
    4.0   11.8
    5.0   11.7
    6.0   11.5
    8.0   11.3
    9.0   11.4
   10.0   11.2
   12.0   11.0
   15.0   10.9
   16.0   10.8
   18.0   10.6
   20.0   10.5
```

Fig. 3 Example of produced mask model

It was reported in a previous study that a double difference of carrier signal phases between two sites and two frequencies (L1 and L2) can be employed for the quality check of observation data (Ikeda and Sada, 2012). In the present development, we improved this method by employing the Doppler observables instead of the carrier phase, which is expressed by the equation:

$$D_{ub}{}^{L1L2}(t) = D_{ub}{}^{L1}(t) - D_{ub}{}^{L2}$$
$$= \left|\left(D_u{}^{L1}(t) - D_b{}^{L1}(t)\right)\frac{c}{f_{L1}} - \left(D_u{}^{L2}(t) - D_b{}^{L2}(t)\right)\frac{c}{f_{L2}}\right|$$

where $D_u{}^{L1}(t)$ is the Doppler observable of the L1 carrier signal at the positioning site, $D_b{}^{L1}(t)$ is the Doppler observable of the L1 carrier signal at the reference station, $D_u{}^{L2}(t)$ is the Doppler observable of the L2 carrier signal at the positioning site, $D_b{}^{L2}(t)$ is the Doppler observable of the L2 carrier signal at the reference station, c is the speed of light, f_{L1} is the frequency of the L1 carrier signal, and f_{L2} is the frequency of the L2 carrier signal. By producing the double difference between two sites and two frequencies, the following error components are canceled out: satellite orbit error, satellite clock error, atmosphere and ionosphere delay, and receiver clock error, so that multipath information can be detected to apply the quality check of the obtained observation data.

One of the merits of this method is that the satellite visibility information such as the fisheye lens photo, is not required. This means that only the observation data are necessary to apply this method. On the other hand, the demerit of this method is that both reference station and observations with two or more frequencies are required, which is not normal for GNSS devices such as automobile navigation systems and smartphones. In addition, in this development, the threshold value for rejecting invalid observations was specified as 1.5 cm, which was determined in advance based on the results of evaluation observations performed on GSI's grounds.

3.3 Method 3: 3D map method

Instead of the fisheye lens photo, a three-dimensional map (3D map) can be used to produce the elevation cutoff mask model (Miura et al., 2014). Another mask model was produced by using the 3D map data and applied to eliminate the multipath signals. Examples of the 3D map and produced mask are shown in Figs. 4 and 5, respectively.

3.4 Another method developed in this project

A fourth method was also developed in this project. As described in Subsection 3.2, the Doppler observables can be used to detect the multipath signal. In addition, velocity observables obtained from the Doppler frequency measurements are also usable for the multipath mitigation. According to Kubo (2009), for example, the velocity from the Doppler frequency measurements was used to help

resolve integer ambiguities, and the ambiguity fixing performance was improved. However, we found several problems while evaluating this method, and finally decided not to include the results in this paper because the software was still under development and a comparison under the same satellite conditions could not be done.

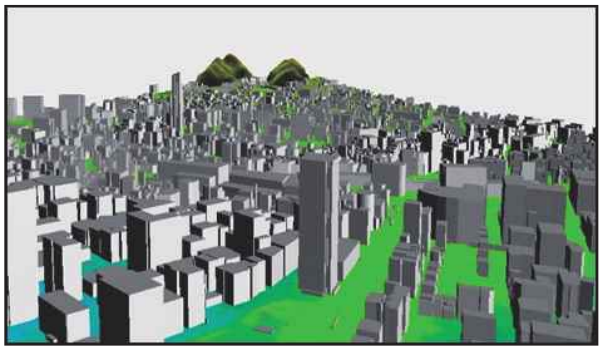

Fig. 4 Example of 3D map

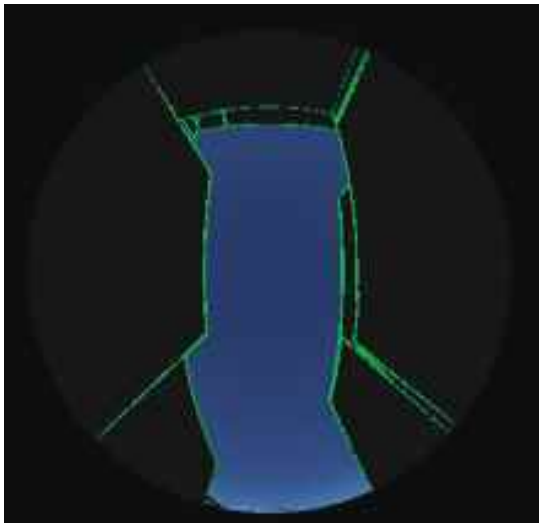

Fig. 5 Example of mask produced with 3D map

4. Trial observation to verify developed methods

To verify the effectiveness of the three multipath mitigation methods introduced above, we conducted trial observations in four areas under urban environments in Kobe City (Fig. 6, Table 1). In addition, four observation sites in each area were picked up considering the different obstacle conditions such as the blocking directions or the materials of the obstacles (Fig. 7). The trial observations were carried out as static positioning not kinematic, and the precision coordinates of the four observation sites were obtained in advance by precise surveying using a Total Station (TS) or network-type RTK. The obtained precision coordinates were used as the reference, and we judged the analysis results of the trial observations to be a fix solution if the difference between them was less than 10 cm for the horizontal direction component.

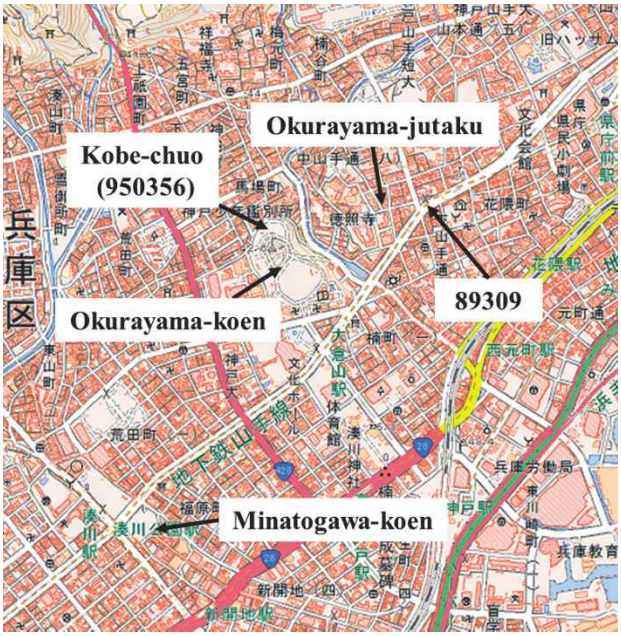

Fig. 6 Distribution map of trial observation areas

Table 1 List of trial observations

Area name	Obstacle condition
Okurayama-koen	Trees, south side
89309	Building, west side
Minatogawa-koen	Building, south side
Okurayama-jutaku	Building, east and south sides

GNSS 12-hour continuous observations were performed at each site on December 21 and 22, 2016 and January 12 and 13, 2017 (four days). Here, the observation time was determined to verify the effectiveness for various satellite constellations especially for receiving of the QZSS signals because only the first QZSS satellite, the signals of which are receivable in Japan for 8 h each day, was available until mid-2017. We performed data processing with baseline analysis between each site and the reference station ‘Kobe-chuo (950356)’ applying each multipath mitigation method. We used the ‘GSILIB’ software developed by GSI for multi-GNSS baseline analysis (Furuya et al., 2014). The configuration of the analysis conditions is listed in Table 2.

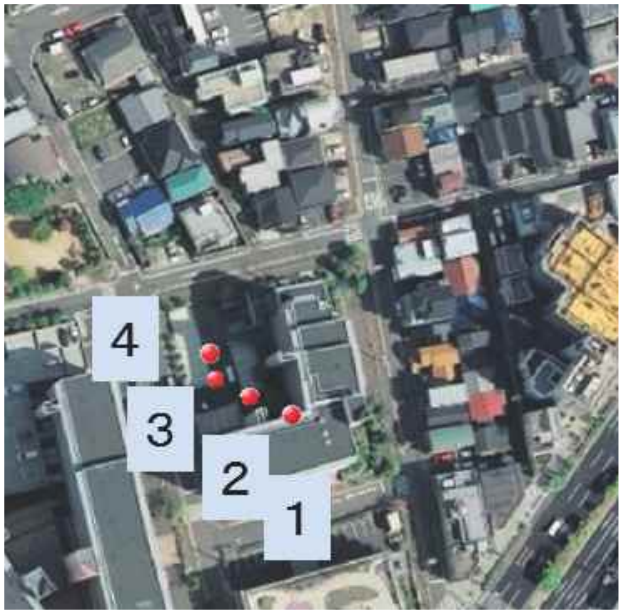

Fig. 7 Distribution map of four observation sites picked up in Okurayama-jutaku area

Table 2 Configurations of GSILIB for trial observations

Items	**Static Mode**	**Kinematic Mode**
Frequency	L1+L2+L5	
L2 Code Priority	L2P(Y)	
Solution Type	Forward	
Default Elevation Mask	15°	
Ionosphere Correction	Broadcast	
Troposphere Correction	Saastamoinen model	
Satellite Ephemeris	Broadcast	
Constellation	GPS, GLONASS, Galileo, QZSS (only one QZSS used)	
Integer Ambiguity Resolution Method	LAMBDA	
Integer Ambiguity Resolution Strategy	Continuous	Instantaneous

The fix rate of each 1-hour observation period was compared as an index of the improvement for each method. Here, the fix rate is the percentage of epochs that satisfy the following conditions for each observation period:

- Ambiguity is resolved for each epoch
- Approximately estimated position for each epoch is less than 10 cm from the reference coordinates for the horizontal direction component

Summarizing the results, the fix rate was improved for all methods except for extremely severe conditions such as huge obstacles. In addition, the 3D map method could not be used for the obstacle condition of tall trees due to the absence of information about the trees in the 3D map that we used. However, the value of the fix rate exhibited a dependency on the observation periods even if the observation data were continuously obtained at the same site. This means that the satellite distribution strongly influences the fix rate under the obstacle condition.

An example of the obstacle condition under which we conducted the trial observations is shown in Photo 2. In this condition, the fix rate values were remarkably improved for all cases of applying the three multipath mitigation methods as described in Fig. 8. The results show that the cases of applying the mask models (fisheye lens photo and 3D map methods) obtained greater improvement and the Doppler observable method case obtained lower improvement. The reason for the lower improvement of the Doppler observable method is that the applied threshold value of 1.5 cm was not suitable for several conditions. This value should be varied depending on the observation condition. Figure 9 shows an example of a wrong judgement of non-line-of-sight satellites that were not rejected by the Doppler observable method. Conversely, a case of good satellites rejected by the Doppler observable method was also confirmed.

5. Evaluation of required precision for mask model

As shown in Section 4, remarkable improvement was obtained for both cases of applying the elevation cutoff mask models (fisheye lens photo and 3D map). This means that the precision of the produced mask model is important for practical use, so we conducted an evaluation of the mask model availability by comparing shifted (biased) models with the original.

Photo 2 Fisheye lens photo at one site in Okurayama-jutaku area

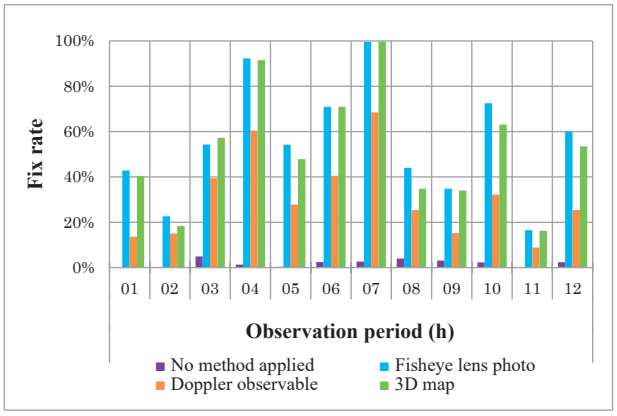

Fig. 8 Results obtained at the site shown in Photo 2

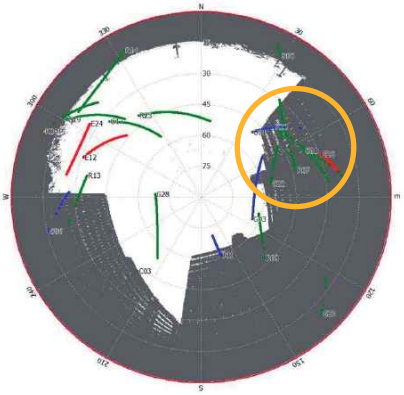

Fig. 9 Combination of mask with fisheye lens photo and results with Doppler observable method. Non-line-of-sight satellites are judged as good (green) within the yellow circle.

The shift values to be added were decided assuming the following items that were considered to originate from practical errors:

- Offset in the vertical direction between the points of the observation and the mask produced
- Offset caused by the tilt of the photo's vertical direction from the zenith
- Offset of north orientation
- Offset caused by the use of a low-precision 3D map

Considering the above, the following biases or error origins were added to the original mask model:

- Uniform elevation bias for all azimuth angles
- Bias originating from the tilt of the photo direction
- Rotation bias to the azimuth angle
- Decimation of interval of azimuth angle (default value of interval: one degree)
- Lower resolution of elevation cutoff mask model

The above biases were added to the original mask model in steps of one degree from −20 to 20 degrees. Here, the tilt to the zenith was applied to the azimuth directions of four types: 0–180, 45–225, 90–270, and 135–315 degrees.

We conducted an evaluation based on the average of the elevation differences between the original and biased mask models for all azimuth directions (hereinafter referred to as "averaged elevation difference"), which is expressed by the equation:

$$\sigma = \sqrt{\frac{1}{N}\sum_{i=1}^{N}\left(el_i - el_{i,0}\right)^2}$$

$$N = \frac{360}{\Delta Az}$$

where $el_{i,0}$ and el_i are the elevation of the original and biased mask model, respectively, at the azimuth direction of Az_i, and ΔAz is the added azimuth step.

We compared the fix rate values of the two cases of no mask model and biased mask model applied. The results are summarized in Fig. 10, which shows that the better fix rate is suddenly reduced at the averaged elevation difference of more than 15 degrees. This means that the applicable averaged elevation difference value should be less than 15 degrees.

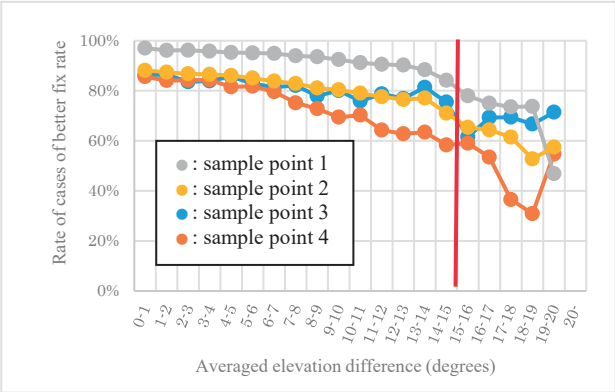

Fig. 10 Results of evaluation of averaged elevation difference

6. Improvement of 3D map method

Since the fisheye lens photo method requires some additional procedures, such as photographing of the fisheye lens photo, calibration of photo distortion, and adjustment of photo orientation, it is not practical for kinematic positioning because the obstacle condition changes every moment. Therefore, the 3D map method is more practical for real-time positioning such as automobile navigation systems and smartphones. However, a priori coordinates are necessary to produce the elevation cutoff mask model using the 3D map, which are not known in advance. In fact, in the case of Section 4, the a priori coordinates were obtained by another positioning (survey) carried out in advance for evaluation of the developed method.

As the next step, we developed a new algorithm to estimate the a priori coordinates simultaneously producing the mask model with the 3D map. A flowchart of this algorithm is depicted in Fig. 11. Iteration of the coordinates estimation (positioning) and mask production using the estimated coordinates is implemented, and full agreement of the list of the used satellites is the judgement condition to terminate this iteration.

We demonstrated this new algorithm, and summarized the results together with the other results in Table 3. Compared with the ideal case in which the actual coordinates were applied, the new algorithm result for the fix rate is worse, but it is much better than the case in which no method is applied. Thus, this algorithm can be used to improve the multipath mitigation.

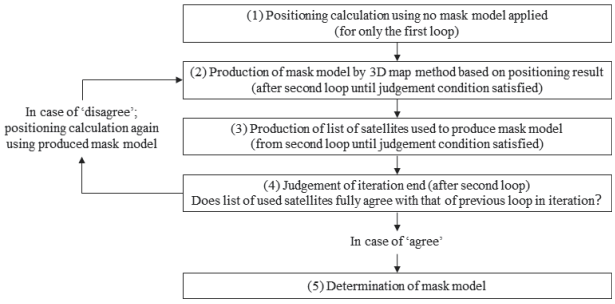

Fig. 11 Algorithm of a priori coordinates estimation and mask model production

Table 3 Comparison of results from new algorithm and others

	New algorithm applied	**Actual coordinates applied**	**No method applied**
Fix rate	57.8%	84.5%	19.5%
RMS [E-W]	0.0121 m	0.0126 m	0.0159 m
RMS [N-S]	0.0057 m	0.0070 m	0.0079 m
RMS [U-D]	0.0409 m	0.5148 m	0.5159 m

7. Verification in urban environments

Based on the developed algorithm, we improved the 3D map method, and conducted verification observations in various obstacle conditions under urban environments simulating kinematic positioning like a rover. Figure 12 shows the distribution map of the route of the kinematic positioning and static observations. This route was determined along a sidewalk located at a site with various obstacles, including tall buildings, shopping areas, dense residential areas, and so on. On the other hand, 23 static sites, on which static observations were performed for 5 min, were chosen from public reference points and the observation sites used in Section 4.

The observations on the route shown in Fig. 12 were carried out three times on December 26 and 27, 2016 changing the observation time to obtain the data under various satellite distribution conditions. The sampling rate of data acquisition was one second for two frequencies of L1 and L2.

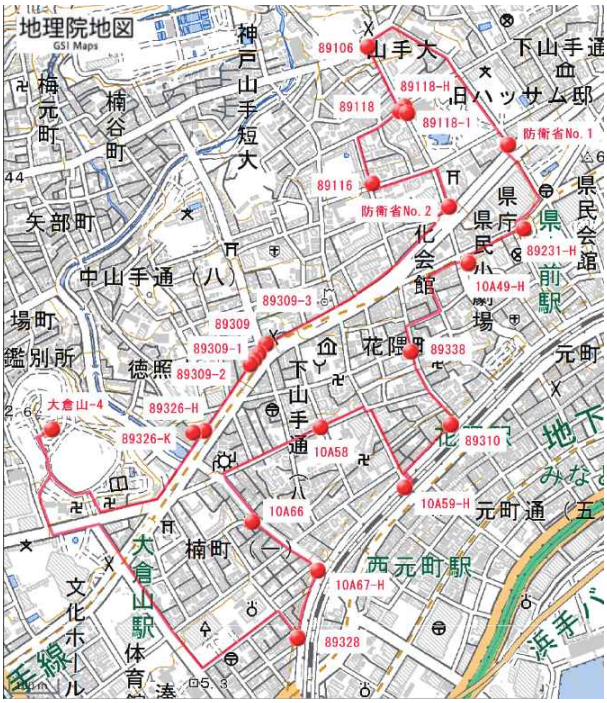

Fig. 12 Route of verification observations. Red dots indicate sites of static observations.

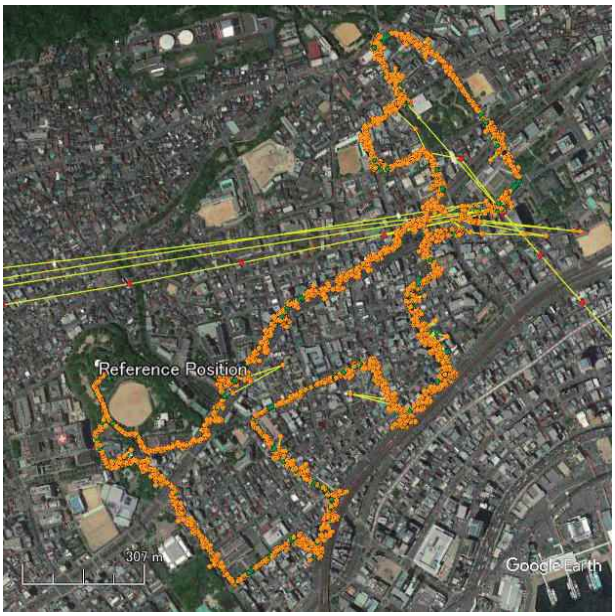

Fig. 13 Distribution of obtained positions plotted on aerial photo (3D map method applied)
● : Fix solution ● : Float solution
● : Single solution

The baseline analysis was performed in three modes: RTK with reference to 'Kobe-chuo (950356),' network-type RTK deploying the Virtual Reference Station near this area, and Precise Point Positioning (PPP).

According to the analysis results, the obtained positions for all analysis modes were plotted on the sidewalk if the sky was fully open. On the other hand, in the case of areas near buildings, some results were scattered, and especially in the areas with tall buildings, the maximum errors were as large as several tens or hundreds of meters. The positions obtained in the RTK mode are plotted on an aerial photo as shown in Figs. 13 and 14. Here, in order to judge the obtained positions as a fix solution, the coordinates that were determined by TS surveying in advance were used as the reference, in the same way as in Section 4. In addition, we introduced the 'satellite visibility rate (SVR)' instead of a percentage of the obstacles in the sky in order to evaluate the effectiveness of the three methods with greater certainty. SVR is defined as the ratio of the satellite-visible sphere that is not masked by obstacles to that of a non-obstacle condition (Fig. 15).

Fig. 14 Distribution of obtained positions plotted on aerial photo (enlarged)
● : Fix solution ● : Float solution

A scatter plot between the SVR and the fix rate is presented in Fig. 16. According to these results, in the case of a SVR of less than 55%, the fix rate values are greatly scattered depending on the multipath mitigation method, which must be influenced by the satellite conditions of the number and distribution in the sky. In addition, in the case

of less than 10% SVR, no improvement is achieved by the three methods. On the other hand, a fix rate of over 80% is achieved when the SVR is more than 55%. This means that the SVR must be more than 55% to apply the three multipath mitigation methods that we developed.

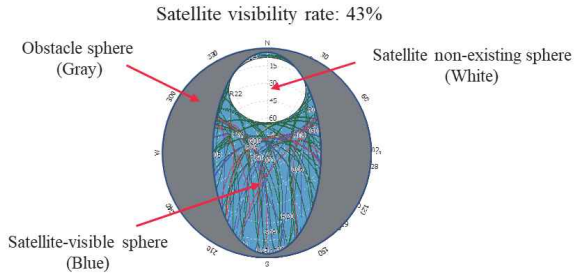

Fig. 15 Conceptual drawing of SVR

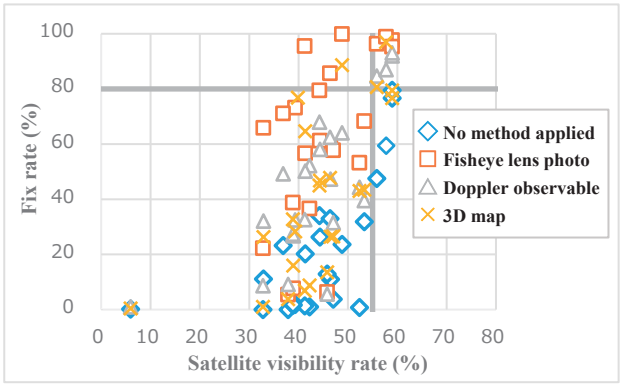

Fig. 16 Scatter plot between SVR and fix rate

Meanwhile, it was also confirmed that this algorithm requires such huge computational resources that a much more powerful computer is necessary for its practical use. To employ this algorithm for real-time positioning such as smartphones, a more efficient algorithm should be developed and implemented.

8. Guidelines for application of developed multipath mitigation methods

Based on the verification results in the previous section, this section summarizes the application guidelines for the developed multipath mitigation methods. The first judgement is whether the SVR is more than 55% or not. If the SVR is over 55%, the multipath mitigation methods can be applied; otherwise, they should not be applied. However, even if the SVR is less than 55%, in a case where the satellite conditions of the number and distribution are suitable, the methods can also be applied. Suitable satellite conditions, however, are not determined yet; this is a future study task.

The second judgement is the applicability of the 3D map method. If the 3D map includes information about the obstacles around the positioning site, the 3D map method can be applied. If not, the fisheye lens photo method can be applied in the daytime (a photo can be taken) and the Doppler observable method can be applied in the nighttime (a photo cannot be taken). A flowchart of the application guidelines for the three multipath mitigation methods is depicted in Fig. 17.

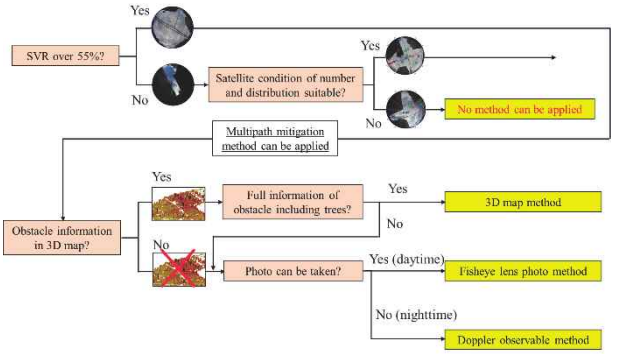

Fig. 17 Flowchart of application guidelines for developed multipath mitigation methods

9. Summary

GSI developed three multipath mitigation methods to improve the accuracy of GNSS positioning under urban environments. To verify the effectiveness of the methods, trial observations were conducted at four sites under different conditions. The results show that except for extremely severe conditions, the fix rate was improved for all three methods, and the application of the elevation cutoff mask model produced with the obstacle information was remarkably effective. A new algorithm was developed to improve the 3D map method assuming kinematic positioning since this method requires no additional procedures except the positioning. According to the results of the verification observations, employing the improved 3D map method, a fix rate of over 80% is achieved if the satellite visibility rate is more than 55%. It is also confirmed that this algorithm requires such huge computational resources that a much more powerful

computer is necessary for its practical use.

This technical development project ended in March 2018. We will publish the multipath mitigation methods and the verification results to promote utilization of the developed methods by other organizations.

Acknowledgements

The authors thank the staff of the contractors, Mitsubishi Space Software Co., Ltd., PASCO Corporation and Hitachi Zosen Corporation for their assistance in this technical development project.

References

Fukuzaki, Y., K. Sakai, Y. Hiyama, T. Furuya, Y. Onaka and K. Miyagawa (2017): Development of Multipath Mitigation Methods to Improve GNSS Positioning Accuracy under Urban Environments, Proceedings of the 9th Multi-GNSS Asia Conference, 18–20.

Furuya, T., K. Sakai, M. Mandokoro and H. Tsuji (2014): Development of Multi-GNSS Analysis Software GSILIB, Journal of the Geospatial Information Authority of Japan, 125, 125–131 (in Japanese).

Ikeda, T and T. Sada (2012): Study on the satellite selection effect using GPS and GLONASS by precise positioning with static state, J. Japan Society of Civil Engineers F3, 69, 2, I98–I109 (in Japanese).

Kubo, N. (2009): Advantage of velocity measurements on instantaneous RTK positioning, GPS Solutions, 13, 4, 271–280.

Miura, S., S. Hisaka and S. Kamijo (2014): GPS positioning with multipath detection and rectification using 3D maps, Int. J. Automotive Engineering, 5, 1, 23–29.

Suzuki, T., M. Kitamura, Y. Amano and T. Hashizume (2011): Multipath mitigation using omnidirectional infrared camera for tightly coupled GPS/INS integration in urban environments, Proceedings of the 24th International Technical Meeting of the Satellite Division of the Institute of Navigation, 2914–2922.

Tsuji, H., Y. Hatanaka, Y. Hiyama, K. Yamaguchi, T. Furuya, S. Kawamoto and Y. Fukuzaki (2017): Twenty-Year Successful Operation of GEONET, Bulletin of the Geospatial Information Authority of Japan, 65, 19–44.